Frequency Response of an Underwater Acoustic Focusing Lens

Songling Huang[a]*, Lisha Peng[b], Hongyu Sun[b], Qing Wang[c], Wei Zhao[b], Shen Wang[b]

[a]State Key of Power System, Department of Electrical Engineering, Tsinghua University, Beijing, 100084, China
[b]State Key Lab. of Power System, Department of Electrical Engineering, Tsinghua University, Beijing 100084, China
[c]Department of Engineering, Durham University, Durham, UK

Corresponding author: Songling Huang (email: huangsling@tsinghua.edu.cn)

This research was supported by the National Key R&D Program of China (Grant No. 2018YFF01012802), National Natural Science Foundation of China (NSFC) (No. 51677093) and National Natural Science Foundation of China (NSFC) (No. 51777100).

ABSTRACT Acoustic lenses composed of metamaterials are used as highly anisotropic subwavelength media and have broad applications in a wide range of industrial areas. As reported in recent research, an acoustic lens composed of a cross-shaped structure can achieve high-intensity 3D focusing in an underwater system. However, the operating characteristics of this lens at different frequencies have not been studied in detail until now. In this work, we studied the focusing performance of a particular acoustic lens at different working frequencies, and the band structure, wave intensity distribution, reflection and transmission coefficients, and refractive index of a unit cell were investigated, as well as the characteristics of the acoustic lens through a simulation and experiment. Errors were minimized in the experiments through reasonable design, and we found that although the wave intensity of a single unit cell decreased as the frequency increased, in the acoustic lens, the intensity of the sound field at its focal point increased with the frequency. The present research provides an improved method for designing acoustic lenses with different working frequencies and can guide nondestructive testing (NDT) and biomedical treatment.

INDEX TERMS Acoustic lens, Metamaterial, Phononic crystal, Frequency, Underwater focusing

1.Introduction

A phononic crystal, also known as an acoustic bandgap material, is a functional composite with a spatially periodic structure [1–5]. Phononic crystals have important applications and research prospects in the fields of noise control, acoustic stealth, filtering, and acoustic focusing control [6–9]. Whether they act as carriers of information or determiners of energy orientation, sound waves are subject to energy attenuation during the propagation process [10–12]. This energy loss is not only due to the expansion of the wave-front but also the acoustic absorption of the propagating medium and the scattering and absorption of scatterers. Therefore, to effectively use sound energy, it is necessary to adopt certain technical methods and equipment to focus sound waves. Furthermore, the focusing of sound field energy has also been used for many purposes, such as nondestructive testing (NDT), medical treatment, and industrial applications [13,14]. Recently proposed methods that enable acoustic focusing include medium reflection focusing, phase control, phased array focusing, and acoustic lens focusing [15]. Acoustic lens focusing is a low-cost, high-efficiency method in practical applications, especially in underwater systems [16]. Since the velocity of sound waves in an acoustic metamaterial is lower than the speed of sound in the medium and the acoustic lens can achieve low-frequency focusing, the size of an acoustic lens can be limited to a desired range [17–21]. Therefore, an acoustic lens constructed using an acoustic metamaterial can effectively focus sound waves. In recent years, the structures, materials, and working conditions of composite metamaterial acoustic lenses have been improved. Ruan et al., in 2019, proposed a 3D underwater acoustic lens using steel rods that could achieve wave focusing, and the structure of a unit cell of this lens was a cross shape (‘‘+”) [22]. In that paper, the focal length along the x-axis determined by experiments and numerical simulations was studied at different frequencies, which led to the conclusion that as the frequency grows, the focal distance is lengthened. However, the reason why the focal length increases was still not discussed in more detail, and error was taken as a possible explanation. Therefore, the performance of the structure pro posed in this paper for a composite acoustic lens should be properly studied at different frequencies. In this way, the function of such an acoustic lens can be further improved.

In this work, a 3D acoustic focusing composite lens in an underwater system was studied at different frequencies. The reflection and transmission coefficients were calculated through the finite element method (FEM) using COMSOL software, and the refractive indexes were obtained. For a unit cell of the composite lens, the sound intensity distributions in the x and y directions were simulated and plotted. Moreover,

the wave intensity magnitudes at different frequencies for acoustic lenses were studied in both simulations and experiments, and the results of both were in good agreement.

2. Method

To study the focusing effect of an acoustic lens and the characteristics of a unit cell, a geometric model is established as shown in Fig. 1. The size of the lens is 156 x 324 x 208 mm3, as shown in Fig. 1(a), and the direction of the three axes is also defined in this figure. Fig. 1(b) shows the geometry of a cross structure with a lattice constant of 12 mm and a rod-edge thickness of 3 mm. In the simulation, the acoustic component in COMSOL is utilized and perfect match layers (PMLs) are applied to the boundaries to minimize the reflection [6]. The meshing for the model is given in Fig. 2 and the meshing parameters are listed in Table 1. The dimensions of the calculation domain are 1600 x 600 x 208 mm^3. Moreover, the mesh in the lens area is refined to reduce numerical errors. A fine tetrahedral meshing is used in the acoustic lens area, and a larger rectangular meshing with more consistent performance is used in the acoustic field radiation area.

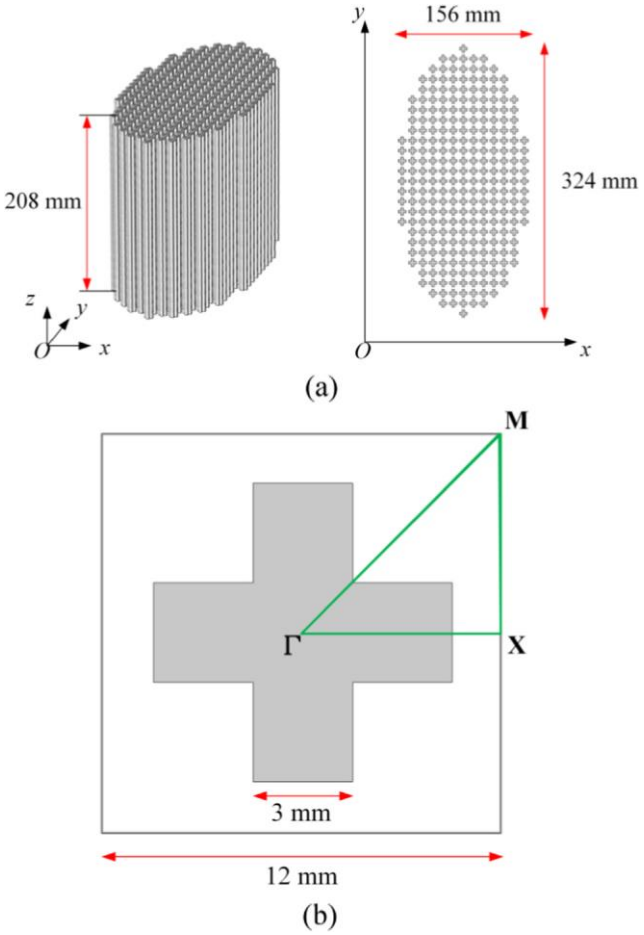

Fig.1. Geometric model of (a) a composite lens, and (b) a unit cell. The Γ-X-M-Γ path is the boundary of the irreducible Brillouin zone.

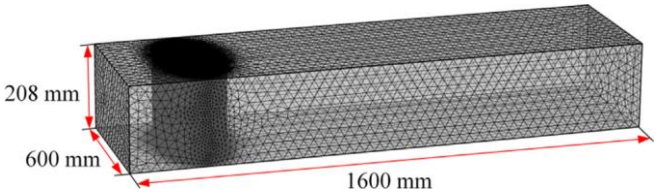

Fig.2. Meshing of the computation domain.

Table 1
Meshing parameters.

Parameter	Value
Number of units	2,4,53,804
Average quality	0.9829
Number of vertices	559,277
Unit volume ratio	7.693 x 10^{-5}

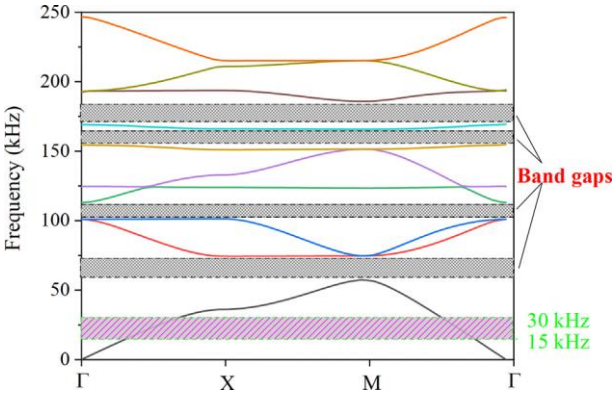

Fig. 3. Band structure of a unit cell along the irreducible Brillouin zone's boundaries.

The band structure (Fig. 3) along the Γ-X-M-Γ path (the green line in Fig. 1(b)) of the irreducible Brillouin zone in the x-y plane is calculated using the finite difference time-domain (FDTD) method [23]. This is a numerical method for directly transforming the wave equation into a differential equation in the time domain and the spatial domain. This equation can calculate complex structures accurately, as well as the nonuniformity, anisotropy, dispersion and nonlinear characteristics of the medium. The band structure can be calculated by the eigen equation:

$$\boldsymbol{u}(\boldsymbol{r}) = \sum_{\boldsymbol{G}\in\boldsymbol{B}} c_n(\boldsymbol{k}+\boldsymbol{G}) e^{i(\boldsymbol{k}+\boldsymbol{G})\cdot\boldsymbol{r}} = e^{i\boldsymbol{k}\cdot\boldsymbol{r}} u_{\boldsymbol{k},n}(\boldsymbol{r}) \quad (1)$$

Where $\boldsymbol{u}(\boldsymbol{r})$ is the displacement vector $\boldsymbol{u}$ at the position vector $\boldsymbol{r}$, $\boldsymbol{G}$ is the inverse vector, $\boldsymbol{B}$ is the periodic lattice in Fourier space, and $\boldsymbol{k}$ is the wave vector. Assuming that the Bloch periodic boundary condition holds, the pattern in the phononic crystal is a set of continuous functions, and n is the band coefficient. In the calculation, the selection of the Bloch vector is not unique. Usually, the unit with the smallest modulus value is selected, and a collection of such units is called the first Brillouin zone (BZ):

$$BZ = \left\{ \boldsymbol{k} \in \boldsymbol{K}^3 : |\boldsymbol{k}| = \min|\boldsymbol{z}|_{\boldsymbol{z}\in[\boldsymbol{k}]} \right\} \quad (2)$$

where $\mathbf{K^3}$ is the Fourier space (also called the wave vector space). Therefore, in Eq. (2), the reciprocal space enclosed by the vertical bisector of the line connecting the origin to

the nearest neighboring inverted point is an irreducible Brillouin zone. Due to the periodicity of the crystal structure, we can obtain the band structure by calculating the boundary wave vectors of the irreducible Brillouin zone. Therefore, the gaps and the range of working frequencies (15 kHz to 30 kHz) are determined, as shown in Fig. 3, and the following simulations and experiments can then be performed.

3. Results and discussion

With the goal of performing a frequency investigation, a unit lattice cell is selected and studied at different frequencies. The reflection and transmission coefficients and the refractive index of a unit cell are calculated as shown in Fig. 4. The transmission coefficient and refractive index decrease with increasing frequency, while the reflection coefficient increases [24]. This situation increases the focal length of the acoustic lens, but the sound field intensity of one cell decreases.

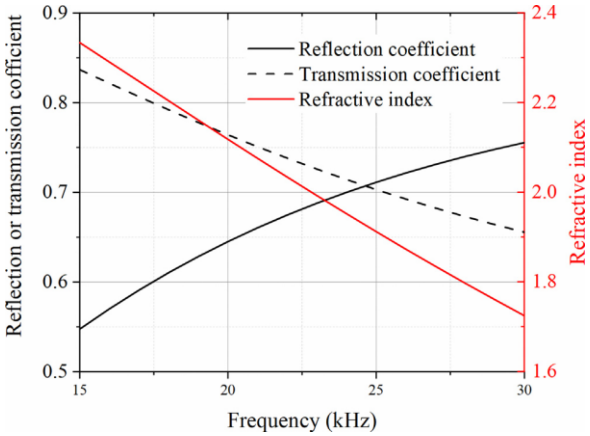

Fig. 4. Relection and transmission coefficients and refractive index of a unit cell.

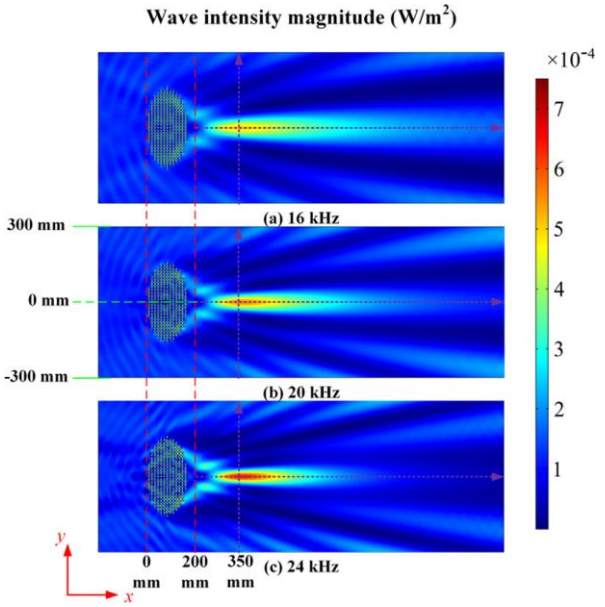

Fig.6. Wave intensity magnitude distribution at different working frequencies: (a) 16kHz, (b) 20kHz and (c) 24kHz. The continuous plane waves are excited and then incident from the left-hand side.

Fig. 5(a) shows the total sound pressure field distribution, and the wave intensity along the x-axis in the incident wave direction is also plotted, as well as the wave intensity along the y-axis in the direction of refraction. Moreover, the continuous plane waves are excited and then incident from the left-hand side. Fig. 5(b) shows that the intensity magnitude I_{mag} along the x-axis decreases with increasing frequency and drops faster as it approaches the boundary of the cross structure.

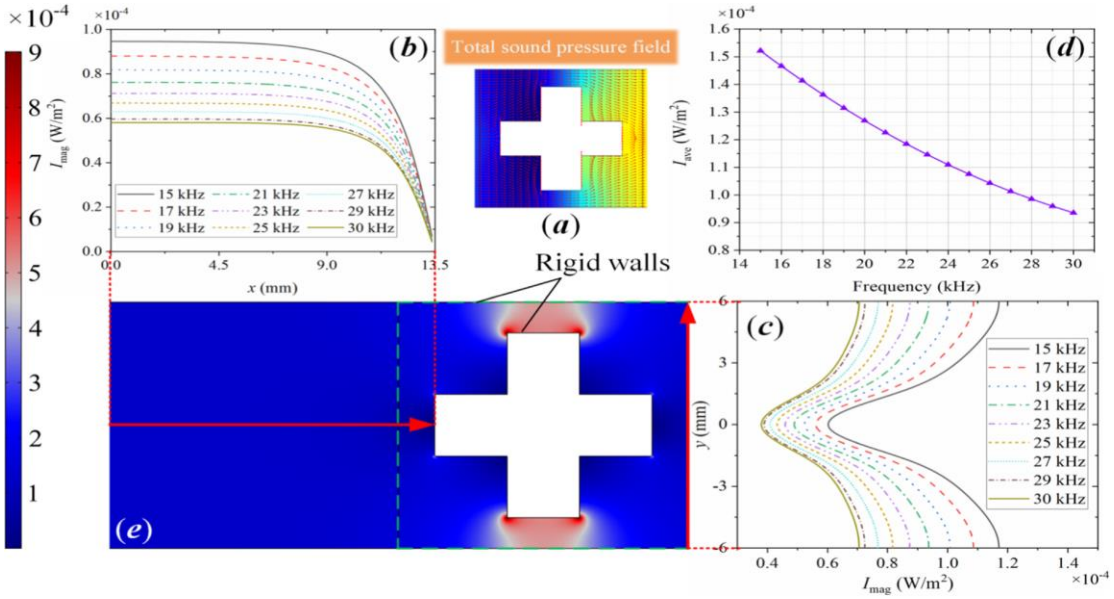

Fig. 5. Simulation results of a unit cell with a cross structure using COMSOL: (a) is the total sound pressure field, (b) is the wave intensity distribution along the x-direction in the center of the cell, (c) is the wave intensity distribution along the y-direction at the refractive boundary of the cell, (d) is the average wave intensity of the cell, and (e) is the sound intensity magnitude distribution. In (e), the plane wave is incident from the left, with a radiation condition on the right hand side. Rigid walls are used for the boundary of the cross structure and the boundaries above and below the calculation area. The area inside the green dashed line denotes a single unit cell. (For interpretation of the references to colour in this figure legend, the reader id referred to the web version of this article.

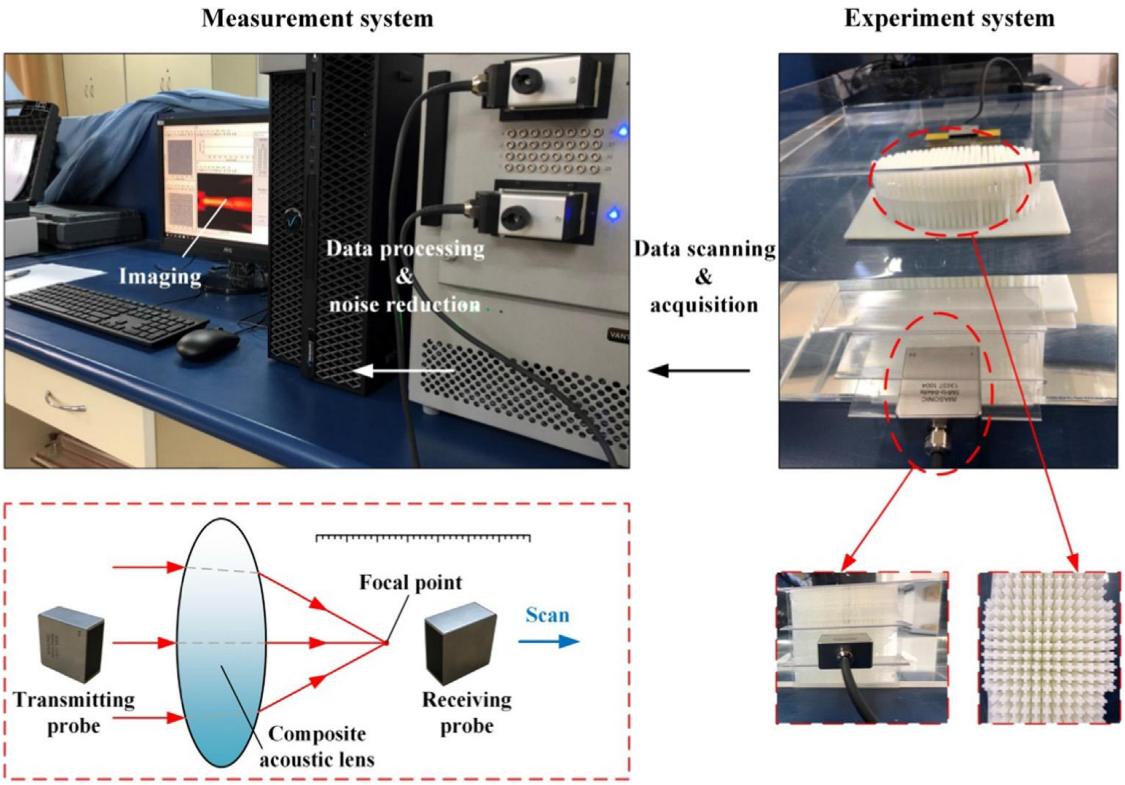

Fig.7. Configurations of the experiment configuration and measurement systems. The water level is slightly below the top surface of the acoustic lens to avoid unobstructed propagation of acoustic waves.

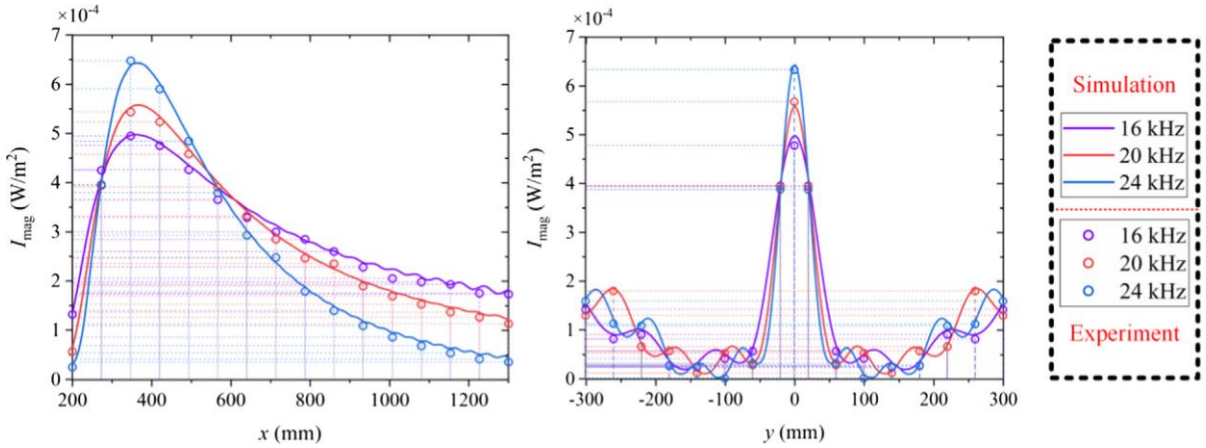

Fig.8. Intensity distribution along the *x*- and *y*- direction. The lines represent simulation results, and the hollow circles represent experimental results. Both results are normalized to their maximum values.

Fig. 5(c) shows that the intensity magnitude decreases with increasing frequency, and the closer to the center, the lower the sound wave intensity. Therefore, in a phononic crystal of this structure, a higher frequency results in a lower average sound field intensity I_{ave} (Fig. 5(d)).

The focusing characteristics exhibited by a composite acoustic lens are mainly achieved by a specific combination of unit cells, and therefore, it is necessary to obtain the relationship between the focusing characteristics of the acoustic lens and the working frequency through simulation. Fig. 6 shows the wave intensity magnitude at three working frequencies, 16 kHz, 20 kHz and 24 kHz, which are in the range of predetermined working frequencies (15 kHz-30 kHz). We set the lens edge of the incident wave side to the coordinate origin of the *x*-axis and the center of the acoustic lens to the origin of the y-axis. It is clearly seen that the peak of wave intensity magnitudes at the focal points increases with the frequency, which reaches 7.5 x 10^{-4} W/m^2 in the study (Fig. 6(c)).

To validate the simulation results, the experiment aims to measure the acoustic wave intensity after passing the lens (see Fig. 7). The experimental configuration includes the experimental and measurement systems. In the experiment, the 3D-printed material of the lens is a composite material, a mixed material of PLA (polylactic-acid) and metal powder, and its acoustic impedance is approximately 9.5x 10^6 kg/(m^2·s). The transmitting transducer (placed 200 mm from the composite

lens in the *x*-direction) has 64 channels and can transmit ultrasonic waves in any direction at a wide range of frequencies (only the center channel is utilized to act as a point source); another transmitting transducer (also called the receiving transducer) can receive ultrasonic waves from all directions. To measure the acoustic field at different points, 16 scans along the *x*-direction with 100-mm gaps, and 6 scans along the *y*-direction with 100-mm gaps are performed. The data received by each channel are then transmitted to the host controller. Additionally, filtered tap water is used as the host medium in the tank, so for the probes in this experiment, water is selected as the officially specified impedance-matching medium; therefore, the best measurement results can be otained in an underwater system in this work. In the measurement, the received data must be processed on a computer (using MATLAB) and then shown on a display window. It is worth mentioning that the data processing and image display processes can be freely available programming. Furthermore, all the data should be obtained by scanning in the entire wavefield area, so a single measurement with a 64- channel probe is not enough. Therefore, the entire measurement area must first be scanned to obtain all the required data, and then the image can be fully displayed.

Subsequently, the experiment and simulation results are shown in Fig. 8 for the same conditions. The distribution of the wave intensity along the x-axis is shown in Fig. 8(a) and (b) shows the wave intensity along the *y*-axis. The focal length decreases slightly when the operating frequency reduces in Fig. 8(a) [22], and the wave intensity magnitudes also decrease. Although a single unit cell's average sound field intensity Iave decreases with frequency (see Fig. 5(d)), simulation results indicate that most of the energy loss occurs behind the focal point's position (Fig. 8(a)). Therefore, this composite acoustic lens can operate within a certain frequency range, and low frequencies can reduce the sound intensity.

Note that the focal lengths at different frequencies are nearly the same in the simulation and the experiment, and there is almost no error in the focal length [22]. This is because in the experiment, the acrylic plate on the top of the rods is removed, and the bottom plate is designed to be as small as possible to minimize edge diffraction. Furthermore, the position of the sound source is set to be relatively close (200 mm) to the lens, so most of the energy passes through the middle of the lens, thus avoiding the reflection of the top and bottom surfaces. Fig. 9(a–c) are experimental images (also discussed in our previous studies) [25,26], and we smoothed the data so that it can be displayed in high resolution. Since the difference of parameters between numerical and experimental models are minimized in this work, and we also tried to reduce measurement errors, Fig. 8(a, b) show good agreement.

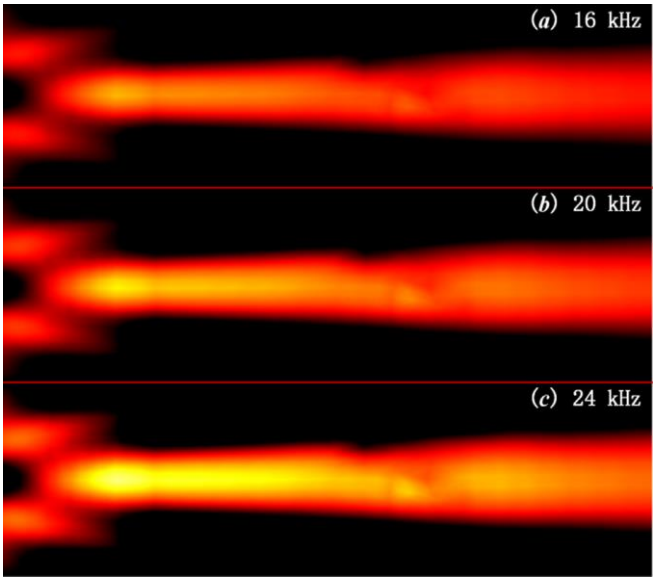

Fig.9. Experiment images at working frequencies of 16kHz, 20kHz, and 24kHz.

4. Conclusions

To conclude, we studied new composite acoustic lenses with ‘‘+”-shaped cells at different working frequencies. A simulation and experiment in an underwater system are carried out in this work and show good agreement, as measurement errors are minimized. We find that although the wave intensity of a single unit cell decreases as the frequency increases, in an acoustic lens, the intensity of the sound field at its focal point increases with frequency. This is because most of the energy loss is in areas far from the focal point. Moreover, the reason why the focal length decreases with the increasing working frequency is that the value of the refractive index is inversely proportional to that of the frequency. We expect that the results of this paper will provide a new design methodology for the improvement of underwater acoustic focusing lenses.

References

[1] Ma, G, Sheng P. Acoustic metamaterials: From local resonnces to broad horizons. Sci Adv 2016; 2: e1501595.
[2] A. Sukhovich, B. Merheb, K. Muralidharan, J. O. Vasseur, Y. Pennec, P.A. Deymier, and J. H. Page, “Experimental and theoretical vidence for subwavelength imaging in phononic crystals,” Physical review letters, vol.102, p.154301
[3] Su, X, Norris A, Cushing C, Haberman M, Wilson P. Broadband focusing of underwater sound using a transparent pentamode lens. J Acoust Soc Am 2017;141:4408.
[4] Climente A, Torrent D, Sánchez-Dehesa J. Sound focusing by gradient index sonic lenses. Appl Phys Lett 2010; 97:104103.
[5] Popa B, Cummer SA, Design and characterization of broadband acoustic composite metamaterials. Phys Rev B 2009;80.2009-01-01
[6] Zigoneanu L. Popa B, Starr AF, Cummer SA. Design and measurements of a broadband two-dimensional acoustic metamaterial with anisotropic effective mass density. J Appl Phys 2011; 109:054906.
[7] L. Wu and L. Chen, “Acoustic band gaps of the woodpile sonic crystal with the simple cubic lattice,” Jourbal of Physics D: Applied Physics, vol. 44, p.045402
[8] M. Kafesaki, M. M. Sigalas and N. García, “Frequency modulation in the transmittivity of wave guides in elastic-wave band-gap materials,” Physical review letters, vol. 85, pp.4044.
[9] J. V. Sánchez-Pérez, D. Caballero, R. Mártinez-Sala, C. Rubio J. Sánchez-Dehesa, F. Meseguer, J. Llinares, and F. Gálvez, “Sound Attenuation by

a Two-Dimensional Array of Rigid Cylinders," Physical Review Letters, vol. 80, pp.5325.
[10] D. Lu and Z. Liu, "Hyperlenses and metalenses for far-field super-resolutio imaging," Nature Communications, vol. 3, 2012.
[11] Zhu J, Christensen J, Jung J, Martin-Moreno L, Yin X, Fok L et al, A holey- structured metamaterial for acoustic deep-subwavelength imaging. Nat Phys 2011; 7:52-5.
[12] Kaina N, Lemoult F, Fink M, Lerosey G. Negative refractive index and acoustic superlens from multiple scattering in single negative metamaterials. Nature 2015; 525:77-81.
[13] J.X.C., L. I. and Khuri-Yakub, "Surface Micromachined Capacitive Ultrasonic immersion Transducers X. C. Jin, I. Ladabaum, B. T. Khuri-Yakub," IEEE Transactions on Ultrasonics, Ferroelectrics, and Frequency Control, vol. 45, pp. 678-890, 2002.
[14] Chang TC, Weber MJ, Wang ML, Charthad J, Khuri-Yakub BPT, Arbabian A. Design of tunable ultrasonic receivers for efficient powering of implantable medical devices with reconfigurable power loads. IEEE Trans Ultrason Ferroelectr Freq Control 2016; 63:1554-62.
[15] Tseng VF, Bedair SS, Lazarus N. Phased array focusing for acoustic wireless power transfer. IEEE Tarns Ultrason Ferroelectr Freq Control 2018; 65:39-49.
[16] Yang J, Tang YF, Ouyang CF, Liu XH, Hu XH, Zi J. Obsevation of the focusing of liquid surface waves. Appl Phys Lett 2009;95:094106.
[17] Yang X, Yin J, Yu G, Peng L, Wang N. Acoustic superlens using Helmholtz-resonator-based metamaterials. Appl Phys Lett 2015,107:193505.
[18] Alagoz S, Kaya OA, Alagoz BB. Frequency-controlled wave focusing by a sonic crystal lens.Appl Acoust 2009; 70:1400-5.
[19] Martin TP, Nicholas M, Orris GJ, Cai L, Torrent D, Sánchez-Dehesa J. Sonic gradient index lens for aqueous applications. Appl Phys Lett 2010; 97:113503.
[20] Y. Li, G. Yu, B. Liang, X. Zou. G. Li, S, Cheng, "Three-dimensional Ultrathin Planar Lenses by Acoustic Metamaterials, "Scientific Reports, vol. 4, 2015.
[21] Shen C, Xu J. Fang NX, Jing Y. Anisotropic complementary acoustic metamaterial for cancelling out aberrating layers. Phys Rev X 2014; 4:041033.
[22] Yongdu R, Xu L, Zhenyu W, Titao W, Yu D, Fengzhong Q, et al. 3-D underwater acoustic wave focusing by periodic structure. Appl Phys Lett 2019; 114:081908.
[23] Su XX, Wang YF, Wang YS. Effects of Poisson's ratio on the band gaps and defect states in two-dimensional vacuum/solid porous phononic crystals. Ultrasonics 2012;52:255-65.
[24] Fokin V, Ambati M, Sun C, Zhang X, Method for retrieving effective properties of locally resonant acoustic metamaterials. Phys Rev B 2007; 76. 2007-01-01.
[25] Sun H, Wang S, Huang S, Peng L, Wang Q, Zhao W. etal. 3D focusing acoustic lens optimizatio method using multi-factor and multi-level orthogonal test designing theory. Appl Acoust 2020;170:107538.
[26] Sun H, Wang S, Huang S, Peng L. Wang Q, Zhao W. Design and characterization of an acoustic composite lens with high-intensity and directionally controllable focusing. Sci Rep 2020; 10:1469.